Hexagonal Crystal Structure of the A-DNA Octamer d(GTGTACAC) and Its Comparison with the Tetragonal Structure: Correlated Variations in Helical Parameters†

Sanjeev Jain,‡,§ Gerald Zon,∥ and Muttaiya Sundaralingam*,‡,⊥

Department of Biochemistry, College of Agricultural and Life Sciences, University of Wisconsin—Madison, Madison, Wisconsin 53706, and Applied Biosystems, Foster City, California 94404

Received August 28, 1990; Revised Manuscript Received November 28, 1990

ABSTRACT: The alternating DNA octamer d(GTGTACAC) has been grown in a novel hexagonal crystal form. The structure has been determined and refined to a 2-Å resolution, with 51 water molecules. The A-DNA conformation is a variant of that observed for the tetragonal form of the same sequence (Jain et al., 1989) containing a bound spermine. The crystals belong to the space group $P6_122$, $a = b = 32.40$ Å and $c = 79.25$ Å, with one strand in the asymmetric unit. The new hexagonal structure was solved by rotation and translation searches in direct space and refined to a final R value of 12.7% by using 1561 unique reflections greater than $1.5\sigma(I)$. The electron density clearly shows that the penultimate A7 sugar had flipped into the alternative C2′-endo pucker. This dent in the molecule can be attributed to close intermolecular contacts. In contrast, in the tetragonal structure, the DNA is distorted in the central TA step, where the A5 backbone bonds C4′–C5′ and O5′–P assume trans conformations. The hexagonal double helix more closely resembles the fiber diffraction A-DNA, compared to the tetragonal form. For instance, the tilt angle is higher (16° vs 10°), which is correlated with a larger displacement from the helix axis (3.5 vs 3.3), a lower rise per residue (2.9 vs 3.2), and a smaller major-groove width (6.1 vs 8.7), thus indicating that the variations in these global helical parameters are correlated. The propeller twist angles in both forms are higher for the G-C base pairs (15.3°, 12.14°) than for the A-T base pairs (10.8°, 9.1°), which is the reverse of the expected order. Unlike the tetragonal structure, the hexagonal crystal structure interestingly does not contain a bound spermine molecule. Our analysis reveals that the conformational differences between the tetragonal and hexagonal forms are not entirely due to the spermine binding, and crystal packing seems to play an important role.

The ensemble of X-ray structures of individual nucleotides and oligonucleotides has confirmed that the overwhelming majority of nucleotides adopt the two preferred conformations, C2′-endo and C3′-endo (Sundaralingam, 1969), and there is more variability in the C2′-endo nucleotide conformation due to the inherent flexibility of the C2′-endo sugar pucker (Sundaralingam, 1982). The minor conformation of syn is observed primarily in the left-handed Z-DNA (Wang et al., 1979) and base-pair mismatches (Brown et al., 1986). Thus, while the X-ray structures of oligonucleotides are consistent with the "rigid nucleotide" concept (Rubin et al., 1972; Sundaralingam, 1973), they also demonstrate that within the bounds of the preferred conformation of the nucleotide there is latitude to allow significant variability in the DNA double helix, as determined by the wide range of helical parameters observed in the various oligonucleotide structures. So far, most of the heterogeneity in DNA structure has been ascribed to the sequence of the oligonucleotides. Recently however, there has been a surge of interest on the role of the crystalline environment in determining DNA conformation (Di Gabriele et al., 1989; Jain & Sundaralingam, 1989; Shakked et al., 1989).

Table I: Crystallographic Data for d(GTGTACAC)

parameter	hexagonal	tetragonal
a (Å)	32.40	42.43
b (Å)	32.40	42.43
c (Å)	79.25	24.75
vol (Å^3)	72048	44558
vol/base pair (Å^3)	1501	1392
asym unit	1 strand	1 strand
Z	12	8
space group	$P6_122$	$P4_32,2$

Earlier we reported the structure of the octamer d(GTGTACAC) in the tetragonal form, with a bound spermine (Jain et al., 1989). We have now crystallized the same sequence in a novel hexagonal form. The structural analysis reveals that the DNA duplex in the hexagonal crystals differs significantly when compared with the tetragonal crystals. Most of the differences in the two crystal forms are due to the distortions in certain nucleotides that seem to arise from differences in the intermolecular contacts. The distortions or deformations observed emphasize the plasticity of the DNA molecule, which is a result of the inherent flexibility of the individual nucleotides themselves (Sundaralingam, 1969). In this paper we report the details of the crystallographic analysis of the hexagonal form and compare its structure with the tetragonal form.

† This research is supported by Grant GM-17378 from the National Institutes of Health of the USPHS to M.S.

* Author to whom correspondence should be addressed.

‡ Department of Biochemistry, University of Wisconsin.

§ Present address: Department of Biochemistry, St. Louis University School of Medicine, St. Louis, MO 63104.

∥ Applied Biosystems.

⊥ Present address: Department of Chemistry, The Ohio State University, 120 West 18th Ave., Columbus, OH 43210-1173.

0006-2960/91/0430-3567$02.50/0

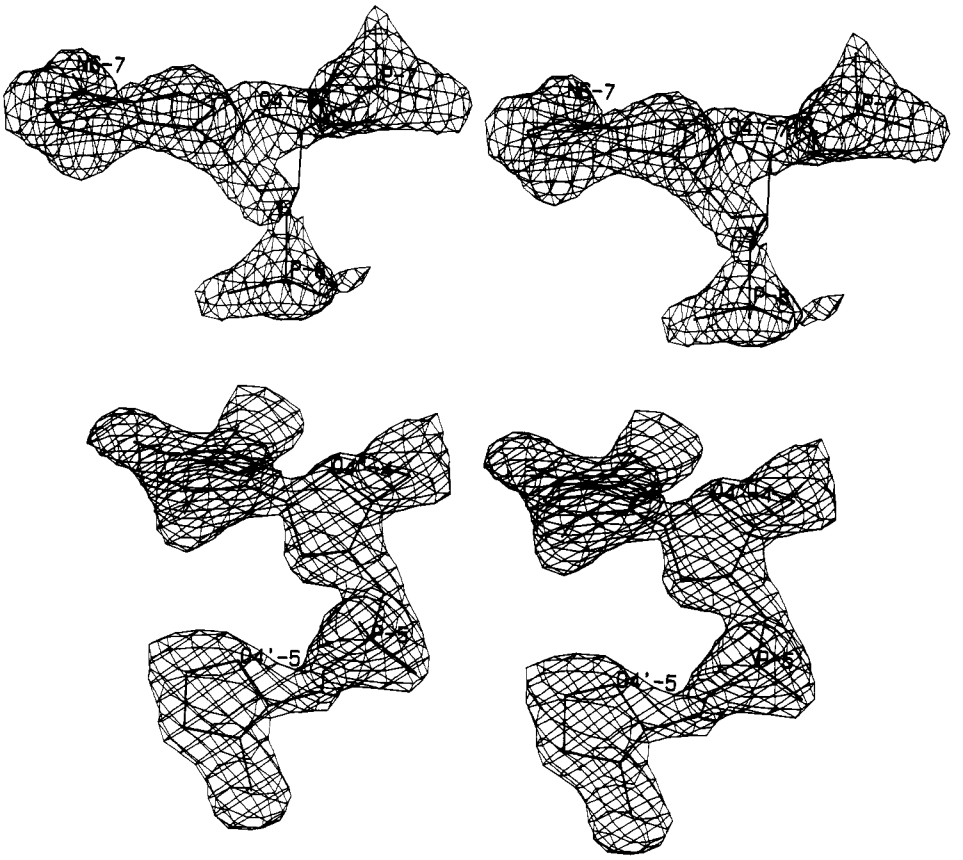

FIGURE 1: Representative sections of electron-density omit maps. (A) The A7 nucleotide in the C2′-endo conformation showing a good fit for the adenine base in the high χ angle and the P atoms of the 5′- and 3′-phosphates at 6.85 Å apart. The sugar C3′ atom is not in the density map. Puckering the sugar into the C3′-endo conformation does not resolve this problem because the accompanying low χ angle for the base and the shorter 3′- and 5′-phosphate separation show considerably poorer fit to the density. (See also Figure 6.) (B) The base T4 and the central sugar–phosphate–sugar backbone segment showing the standard gauche$^+$ conformation for the C4′–C5′ bond and the gauch$^-$ conformation for the O5′–P bond.

Table II: Progress of the Refinement

resolution (Å)	no. of refl[a]	cycles	*R* factor initial	*R* factor final	no. of waters	remarks
7.0–2.94	881	55	41.4	33.9	0	resolution gradually increased from 4.54 to 2.94 Å with a fixed B = 20 Å^2
7.0–2.27	1944	33	32.4	23.5	0	model refitted to $2F_o - F_c$ omit maps and resolution gradually increased to 2.27 Å; a total of 132 reflections between 7.0 and 5.0 Å resolution had a $\sum F_o/\sum F_c$ ratio of 0.74 and were omitted from further refinement
5.0–2.0	2655	20	23.2	21.6	0	extended the data from 5.0- to 2.0-Å resolution and continued refinement with individual B values
5.0–2.0	2655	77	24.1	14.3	70	waters added and model refitted to difference omit maps
5.0–2.0	2655	67	15.1	12.7	101	waters refitted

[a] The number of reflections indicated in this column is for the expanded data set for the lower symmetry space group $P6_1$. The number of reflections given in the text is for the correct space group $P6_122$.

Table III: Refinement Statistics

restraint	no.	RMS deviation	σ	no. deviating $>2\sigma$
distance restraints				8
bonds	304	0.009	0.025	
angle distances	448	0.023	0.050	
phosphate bonds	56	0.050	0.050	
phosphate angles, hydrogen bonds	344	0.054	0.075	
plane restraints	168	0.014	0.030	0
chiral center restraints	48	0.050	0.100	0
nonbonded contacts				
single torsion	4	0.034	0.063	0
multiple torsion	56	0.158	0.063	21
thermal factor restraints				0
sugar–base bond	304	3.83	5.00	
sugar–base angle	448	4.10	5.00	
phosphate bond	56	4.54	5.00	
phosphate angles, hydrogen bonds	344	3.99	5.00	

Materials and Methods

The octamer sequence was synthesized as before by solid-phase phosphoramidite chemistry with a Biosystems automated synthesizer, and the deprotected trityl derivative was purified by using reverse-phase HPLC (Zon, 1990). The crystallization conditions used were the same as those used to grow the original tetragonal crystals by the vapor-diffusion technique, viz., 40% MPD in the reservoir and 2 mM each of $MgCl_2$, spermine, and the DNA duplex in the droplet. Initially no crystals were obtained even after several months. Subsequently, crystals were obtained by seeding with either fragments of the original crystal or the mother liquor. Although the latter gave better crystals, surprisingly they were all found to have a hexagonal lattice. Seeding with hexagonal crystals resulted in more hexagonal crystals. We tried to adjust the crystallization conditions, including the pH, Mg^{2+} ions, spermine, and DNA concentration, but were not successful in obtaining the tetragonal crystals. The hexagonal crystals grew at 4–6

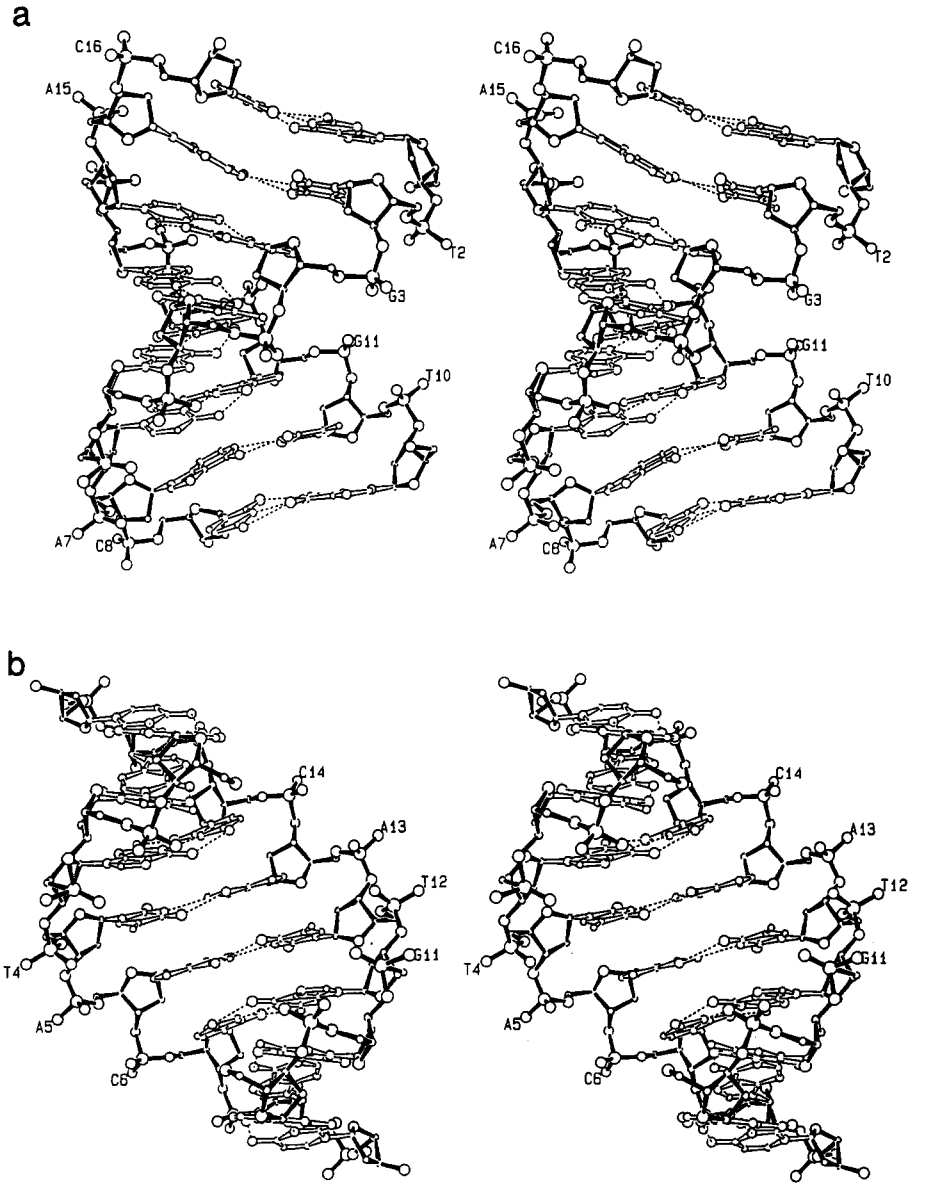

FIGURE 2: Stereopairs showing two views of the hexagonal structure, (a) perpendicular to the dyad axis, showing the deep major and the shallow minor grooves, and (b) down the dyad axis into the major groove. Note the C2′-endo pucker of the A7 and A15 sugars gives the A7-T10 and A15-T2 base pairs a larger base buckle angle than a propeller twist angle.

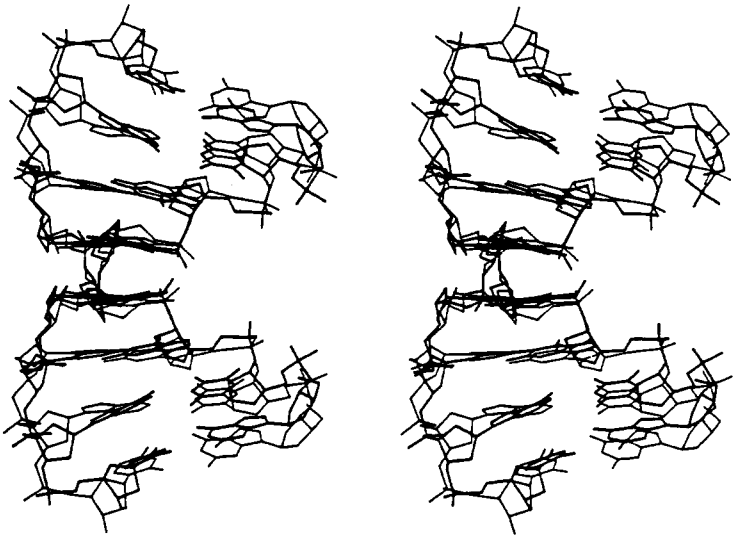

FIGURE 3: Stereopair of the superposition of the hexagonal (thick bonds) and the tetragonal (thin bonds) d(GTGTACAC) structures. The narrower major groove in the hexagonal structure can be clearly seen by the smaller P–P separation across the deep groove.

Table IV: Helical Parameters in Hexagonal and Tetragonal Structures[a]

sequence	tip	inclination	roll	prop. twist	buckle	twist	rise	x-disp
G	8.0	13.7		16.8	11.1			-3.6
	-7.2	11.5		11.3	11.5			-3.2
			-1.9			35.9	2.06	
			6.0			31.3	3.50	
T	-4.0	17.8		10.2	19.4			-3.8
	-6.7	9.0		9.9	1.7			-3.3
			13.2			31.3	3.41	
			10.7			31.4	3.19	
G	0.5	16.1		13.9	9.8			-3.4
	-0.5	9.2		13.5	5.1			-3.1
			6.2			32.3	3.02	
			6.3			36.0	3.05	
T	-2.2	14.7		11.5	1.3			-3.9
	-0.3	10.4		8.3	4.6			-3.2
			12.0			31.6	3.12	
			5.6			28.3	3.13	
A	2.2	14.7		11.5	-1.3			-3.9
	0.3	10.4		8.3	-4.6			-3.2
			6.2			32.3	3.02	
			6.3			36.0	3.05	
C	-0.5	16.1		13.9	-9.8			-3.4
	0.5	9.2		13.5	-5.1			-3.1
			13.2			31.3	3.41	
			10.7			31.4	3.19	
A	4.0	17.8		10.2	-19.4			-3.8
	6.7	9.0		9.9	-1.7			-3.3
			-1.9			35.9	2.06	
			6.0			31.3	3.50	
C	-8.0	13.7		16.8	-11.1			-3.6
	7.2	11.5		11.3	-11.5			-3.2

[a] Parameters for the hexagonal structure are given on the first line; those for the tetragonal structure are given on the second line. Except for the rise and displacement, which are in angstrom units, the rest of the values are given in degrees.

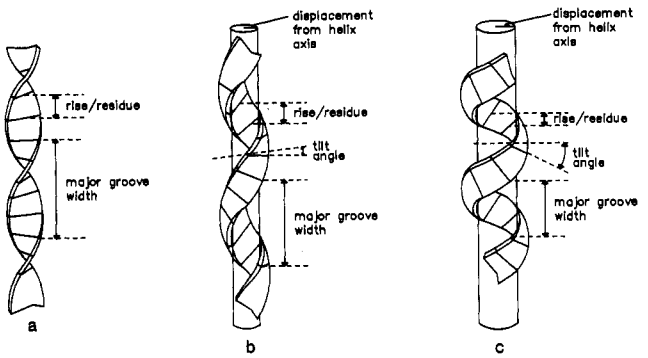

FIGURE 4: The ribbon analogy for DNA shows the B-DNA ↔ A-DNA "continuum"; (a) represents the B-DNA family of conformations, (b) represents the A-DNA in the tetragonal structure that is closer to B-DNA, and (c) represents the hexagonal structure. The ensemble of A-DNA conformations can only approach the B-DNA conformations, and in order to reach and become B-DNA, the A-DNA sugars must switch to C2′-endo. The figures also illustrate schematically the relationship between the base-pair displacement, tilt angle (inclination), rise per residue, and major-groove width.

°C as either truncated bipyramidal or multifaceted structures with uncharacteristic morphology, and the largest measure was 0.2 × 0.3 × 0.4 mm in size. The unit cell parameters and space group for the hexagonal crystals are given in Table I and compared with the tetragonal crystals. Unlike the tetragonal crystals, the hexagonal crystals had lattice dimensions different from any previously known.

Intensity data were collected on one of the larger crystals to a resolution of 2.0 Å by Arndt–Wonacott oscillation photography with two films per film pack, using a GX6 rotating anode X-ray generator. The films were exposed for 5 h, and the intensities were scanned with an Optronics densitometer. After data processing, the hexagonal form had altogether 8156 observations with $I > 1.5\sigma(I)$ and an R(av) of 5.2% in the Laue group of $6/m$. This reduced to 1683 unique reflections with an R(sym) of 2.4% in the Laue group of $6/mmm$; thus 85.7% of the possible reflections were observed. As in the tetragonal structure, here too from considerations of the unit cell volume and the volume occupied per base pair (Table I), it was concluded that the molecules were located on a crystallographic dyad axis.

The structure solution was obtained by an R factor and a correlation coefficient search with the trial models of the octamer sequence in the A-, B-, and Z-DNA conformations. The models were rotated about and translated along each of the two possible crystallographic dyad axes in this space group. A total of 124 reflections in the resolution range of 10–5 Å were used in the search, and both the enantiomeric space groups, $P6_122$ and $P6_522$, were tried. Out of all the possibilities explored, 11 trial solutions gave correlation coefficients higher than 30%, 10 of which were for an A-DNA model in different orientations. Only one B-DNA trial solution and no Z-DNA model satisfied the above criteria. Of the 11, 6 trial solutions, including the one for B-DNA, could be rejected on the basis of severe interpenetrations between symmetry-related molecules. The remaining five A-DNA trial solutions were subjected to an in-house minimization program called RVMIN (Jain, unpublished). This program sequentially refines all six orientational and positional parameters of the molecule to maximize the correlation coefficient. For one of the trial solutions in space group $P6_122$, after five cycles of RVMIN runs, the correlation coefficient jumped to 48%, and the R factor dropped to 40.3%, with less than 2° movement in any of the rotational parameters. For the other four solutions, the correlation coefficient did not increase above 35%. When B- or Z-DNA models were placed in the above best orientation, or when the A-DNA model was placed in the unit cell with $P6_522$ symmetry, there were significant steric clashes between symmetry-related molecules.

A $3F_o - 2F_o$ electron density map was calculated for the best solution, and the A-DNA model was refitted into the density

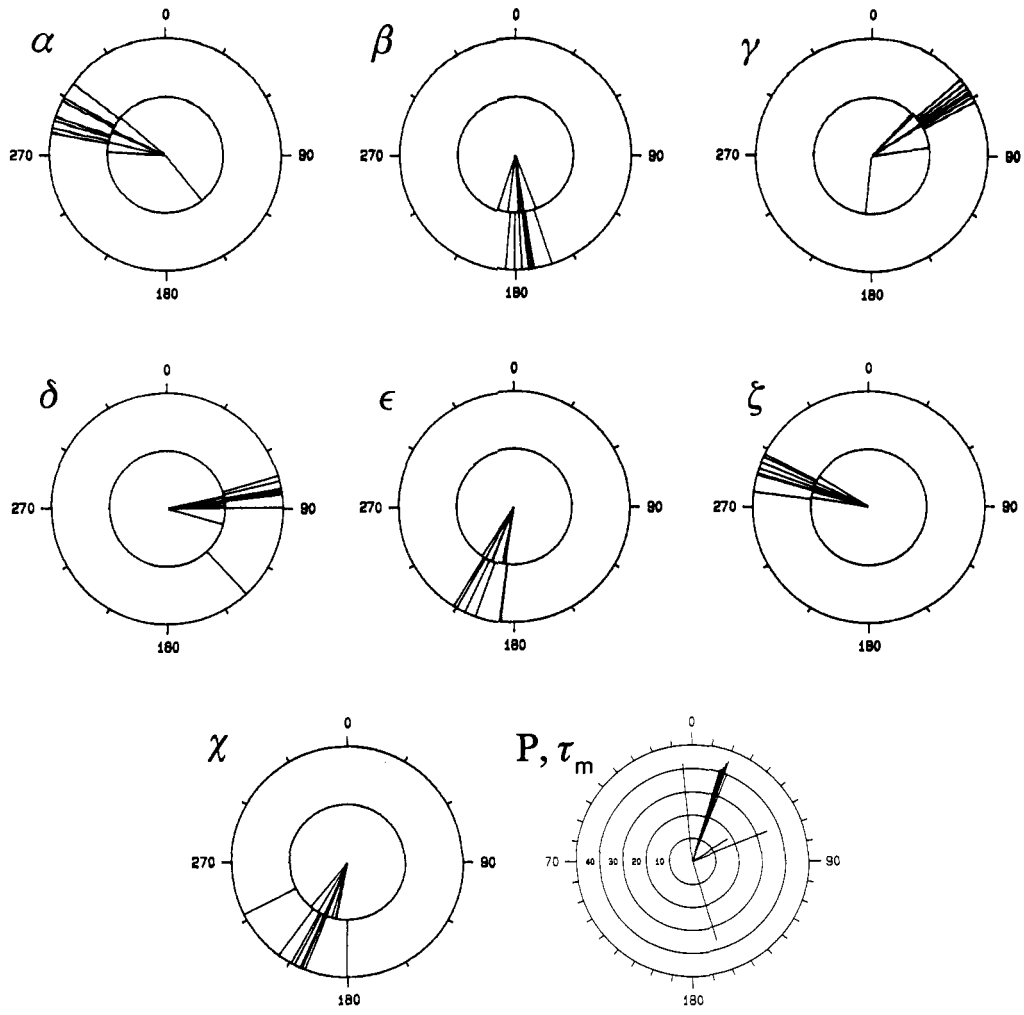

FIGURE 5: Backbone conformation (α–ζ) and glycosyl (χ) angles and pseudorotation P and τ_m values represented in the form of "wheels" for (outer circles) the hexagonal octamer and (inner circles) the tetragonal octamer.

map by using the program FRODO (Jones, 1985) on an Evans and Sutherland PS300 molecular graphics system. This process increased the correlation coefficient to 81.7% and reduced the R factor to 39.2% for the 10–5.0-Å data. With the other trial solutions, the electron density was discontinuous, and refitting the models did not affect the correlation coefficient or the R factor significantly; therefore these solutions were rejected.

After fitting the model to $3F_o - 2F_c$ electron density maps, the structure was subjected to a restrained least-squares refinement with the program NUCLSQ (Westhof et al., 1985). For the refinement, the space group of the crystal was lowered to $P6_1$, the data were expanded to point group 6, and the full octamer duplex was treated as the asymmetric unit. This procedure enabled the introduction of base-pair hydrogen-bonding restraints. In order to keep the two strands of the octamer nearly identical, the dyad operator was introduced as a strong noncrystallographic symmetry element; and after every 20 cycles of refinement, the coordinates of the two strands were normalized to make them identical. The steps in the progress of the refinement are shown in Table II.

Initially, 190 reflections in the 7.0–4.54-Å resolution range were used, and after 70 cycles of NUCLSQ refinement and one round of map fitting by $2F_o - F_c$ "omit maps", the data were slowly expanded to the 7.0–2.27-Å resolution range. We noticed that the 132 low-angle reflections in the 7.0–5.0-Å resolution range had a lower value for $\langle F_o \rangle$ than $\langle F_c \rangle$ with an $(\sum F_o / \sum F_c)$ ratio of 0.74. A very similar problem was encountered in our work on the tetragonal octamer (Jain et al., 1989, and unpublished results) and a plot of $\langle F_o \rangle / \langle F_c \rangle$ vs resolution showed a biphasic curve with the inflection point at 5.0 Å. The cause of this discrepancy remains unclear, but it may be related to the scattering by bulk solvent and the film method of data collection. A similar behavior was also observed by Chambers and Stroud (1977), who scaled the low- and high-angle data using a four-parameter scaling. We also attempted to scale the low- and high-angle data using a four-parameter scaling during the refinement of the tetragonal octamer. After this scaling, five rounds of map fitting and refinement yielded only 19 water molecules in the asymmetric unit, with an R factor of 16% for the 10.0–2.5-Å resolution data. The resulting electron-density maps were somewhat noisy, and the electron densities for many of the water molecules were inconsistent from one round to the next. Therefore, the 132 low-angle reflections below 5.0 Å in the hexagonal structure were omitted in the further rounds of refinement, which included all the data from 5.0–2.0-Å resolution. The clarity of the omit maps was considerably enhanced and allowed a better elucidation particularly of the water sites (Figure 1).

The criteria and method for determing water binding sites in the hexagonal structure were the same as reported previously (Jain et al., 1989). While a total of 51 water molecules were located, there was no evidence of the presence of spermine. This was a surprising result in view of the bound spermine in the tetragonal structure. Several cycles of restrained refine-

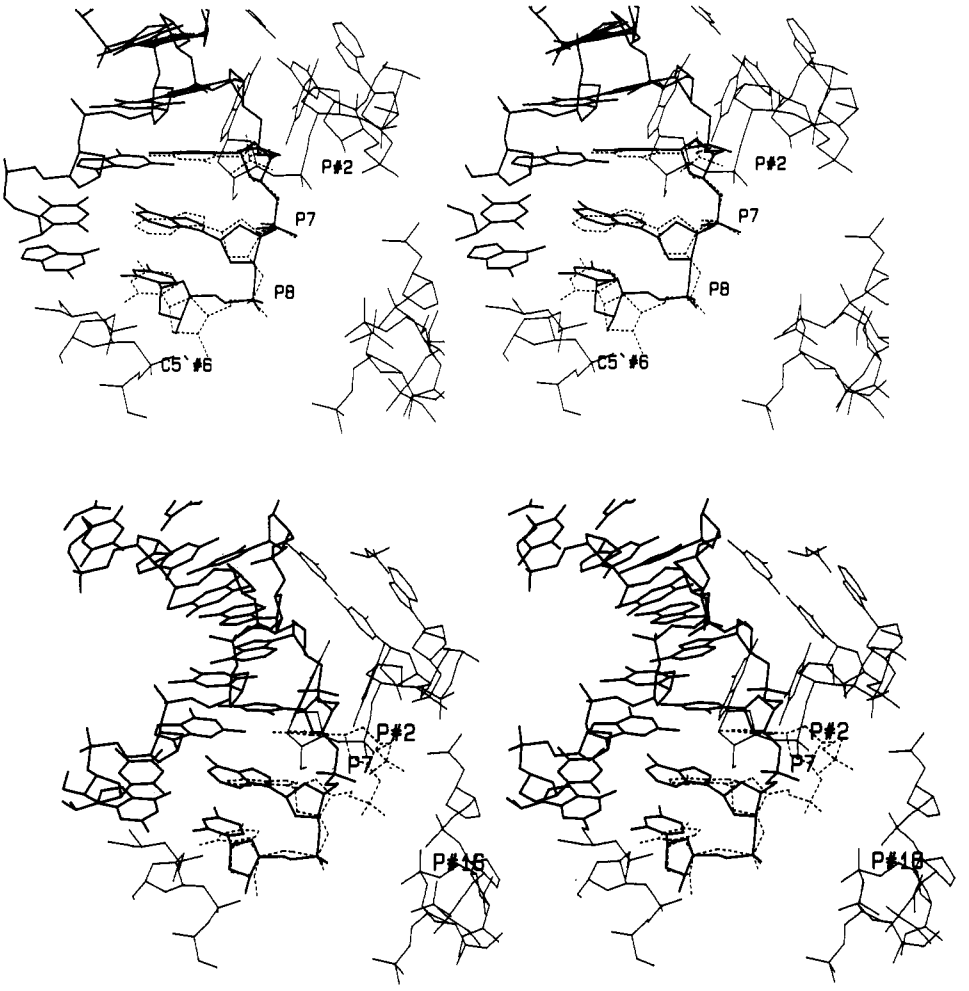

FIGURE 6: Stereoviews illustrating the reason for the flip of the sugar pucker of A7 from C3′-endo to C2′-endo in the hexagonal structure. (A) When the sugar of the sixth residue in the reference molecule (shown in dark lines) is superimposed on that of a trinucleotide with the standard A-DNA conformation (shown in broken lines), the terminal residue C8 does not stack optimally with the symmetry-related molecule below (shown in thin lines) and also leads to close contacts with neighboring molecules. (B) When the sugar of the terminal (C8) residue is superimposed on that of the A-DNA trinucleotide, the direction of the oligonucleotide chain changes markedly, and the P7 phosphate comes into close contact with P2 and P16 of symmetry-related molecules. Parts of three symmetry-related molecules are shown in thin lines, two on the right side and the third below the reference molecule.

ment, varying individual atomic thermal parameters, and model fitting gave a final R factor of 12.7% for the 1561 reflections with $I > 1.5\sigma(I)$. It is interesting that the seven additional water molecules found in the hexagonal form account for the seven non-hydrogen atoms in the asymmetric half of spermine. However, it is important to emphasize that the distribution of the spermine atoms did not all correspond to the water sites. The water molecules appeared in the omit maps at an average height of 2.7σ and distances of 2.3–3.5 Å (av 2.91 Å) from a hydrogen bond acceptor or donor atom. The average thermal parameters (in Å^2) for the phosphates, sugars, and bases were 29, 25, and 21, respectively, and for the water molecules they were between 30 and 73 (av 50). The average and lowest occupancies of waters were 0.86 and 0.52, respectively. The refinement statistics are summarized in Table III. The coordinates and structure factors have been deposited with the Brookhaven Protein Data Bank.

Results and Discussion

Stereoviews of the hexagonal octamer in two orientations are shown in Figure 2. The stubby helix is characteristic of an A-DNA, with a C3′-endo sugar (except at A7), the high tilt of the base pairs, the displaced base pairs from the helix axis, and the deep cavernous (narrow) major groove and shallow (wide) minor groove. Thus the widths of the major and minor grooves are interchanged compared to B-DNA. Further, the phosphate groups line the deep groove and are virtually inaccessible from the narrow-groove side. This feature is particularly emphasized in A-DNA compared to B-DNA.

Global Helical Geometry in the A-DNA of the Hexagonal and Tetragonal Structures. The average base-pair tilt angle and the displacement from the helix axis are 16° and 3.5 Å compared to 10° and 3.3 Å, respectively, in the tetragonal form (Table IV). The major-groove width is only 6.1 Å (vs 8.7 Å) and the rise per residue is 2.9 Å (vs 3.2 Å). On the other hand, the widths of the minor grooves in both structures are nearly the same; for the hexagonal it is 9.6–11.0 Å and for the tetragonal it is 9.7–10.0 Å (see below). These characteristics make the hexagonal structure closer to the classical fiber A-DNA than the tetragonal structure. The tetragonal structure is significantly elongated as seen by the longer P–P separation in the cavernous groove (Figure 3).

Correlated Variations in Helical Parameters: The Ribbon Analogy. The above observations indicate that A-DNA occurs as a family of helices with a continuum of values for many of the helical parameters (Jain et al., 1987; Heinemann et al., 1987; Fairall et al., 1989). The variation in these parameters is correlated. It is found that the displacement and the tile

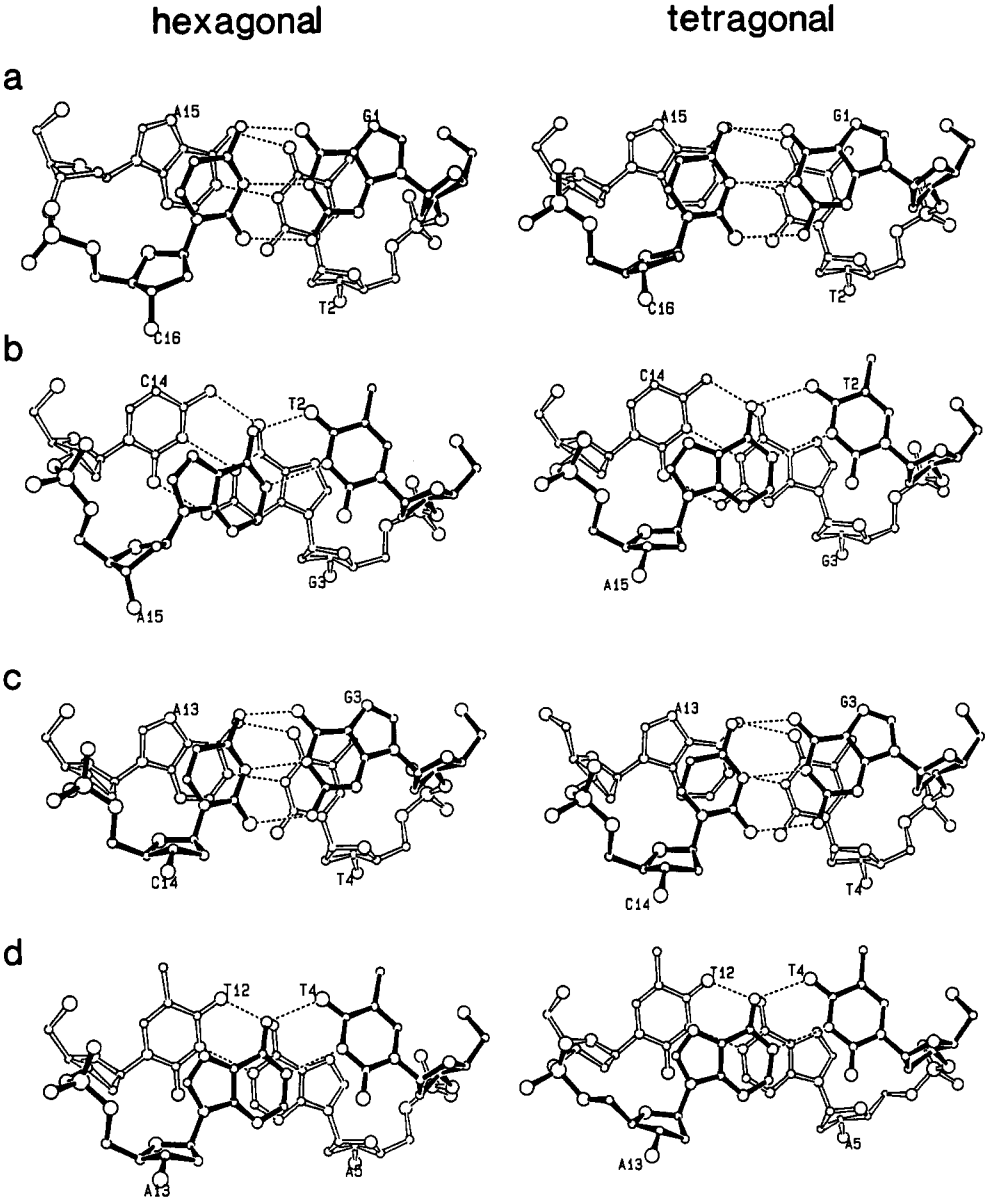

FIGURE 7: Base-stacking geometries in (left) in hexagonal and (right) the tetragonal structures shown as dinucleoside pairs. In spite of significant differences in the backbone and global conformations of the two duplexes, base-stacking interactions are similar.

angle (inclination) (Jain et al., 1987), as well as the tilt angle, the major-groove width, and the rise per residue (Heinemann et al., 1987) are correlated. That is, a high displacement is correlated with a high tilt angle, which increases the major-groove width and decreases the rise per residue. These correlations can be exemplified by the ribbon diagram for DNA (Figure 4). The straight twisted ribbon shown in Figure 4a represents B-DNA, where the horizontal lines represent base pairs that have essentially no tilt and no displacement from the helix axis; i.e., the helix axis runs approximately through the center of the base pair. If the ribbon is wrapped around a rod, as shown in Figure 4b, it would represent A-DNA where the base pairs are tilted and displaced from the helix axis. If the base-stacking distances remain constant in both A- and B-DNA, then due to the tilt, the rise per residue would be reduced in A-DNA. Further, if the diameter of the rod is increased, but the number of residues per turn is maintained, then the ribbon will have to be wrapped more tightly. This would mean the tilt angle will increase and the rise per residue will decrease, resulting in narrowing of the major-groove width. In this analogy, the hexagonal structure will be represented by Figure 4c where the base-pair displacement, tilt, etc. are further emphasized. The ribbon analogy also explains the constancy of the minor-groove width for the A-DNA's because it is represented by the width of the ribbon itself.

Backbone Conformation and Distortions in the DNA Duplex. The sugar–phosphate backbone (α–ζ) and the sugar–base glycosyl (χ) torsion angles (IUPAC–IUB, 1983), including the pseudorotation phase angle (P) and amplitude of puckering (τ_m) of the sugars (Altona & Sundaralingam, 1972), are compared for the hexagonal and tetragonal structures in Figure 5. In general, the nucleotide units adopt the C3′-endo sugar pucker, the anti glycosyl conformation, and the gauche$^+$ conformation about the C4′–C5′ bonds. The ester P–O bonds adopt the usual gauche$^-$ conformations (Sundaralingam, 1969). The exceptions are the flip in one of the sugar puckers at A7 (A15) in the hexagonal form and the extension of the backbone at A5 (A13) with a trans C4′–C5′ and O5′–P in the tetragonal structure. The duplex ends in both structures show deviations that are common (Wang et al., 1982; Haran et al., 1987; Heinemann et al., 1987). The deviations in the internal residues, A7 (A15) and A5 (A13), lead to distortions in the

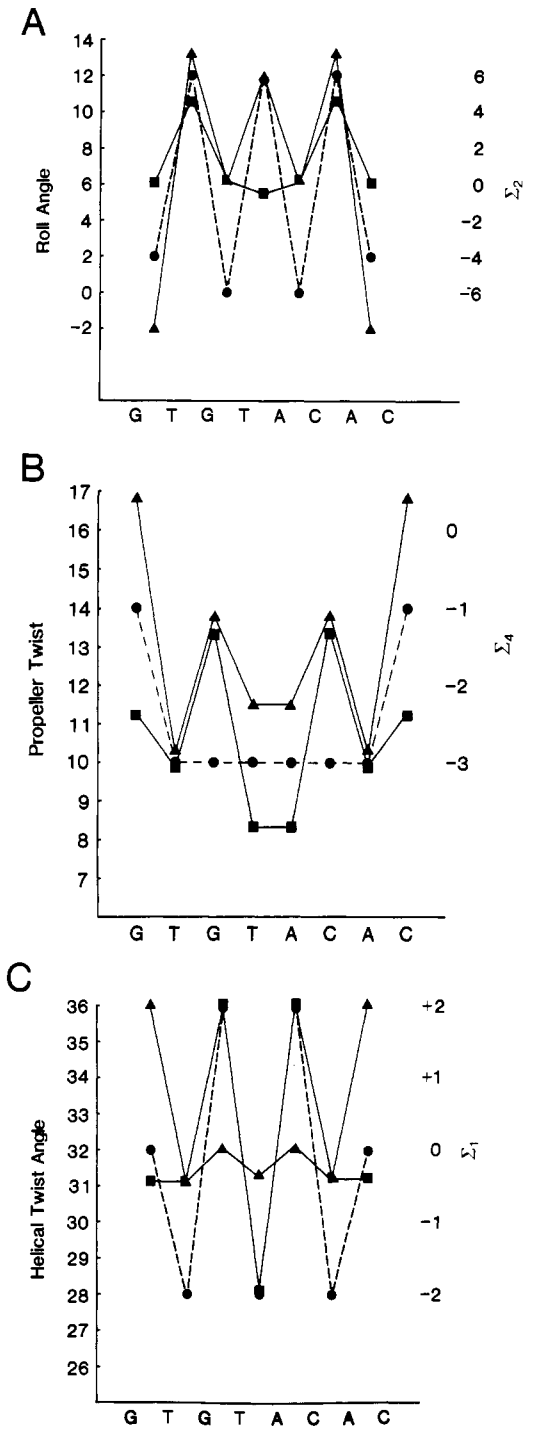

FIGURE 8: Comparison of (A) roll, (B) propeller twist, and (C) twist angles of the (▲) hexagonal and (■) tetragonal structures. (●) The Calladine–Dickerson sum functions (A) Σ_2, (B) Σ_4, and (C) Σ_1 are also plotted.

overall helical structures.

The switch of the sugar pucker of the penultimate residues A7 (A15) from the standard C3′-endo to C2′-endo not only affects the local base-pair (A7–T10) parameters but also perturbs the neighboring base pairs. The C2′-endo pucker is seen for the first time for an inner residue of an A-DNA oligomer. It is very likely that this distortion is brought about by crystal packing. If A7 (A15) were to adopt the standard C3′-endo sugar pucker, there would be clashes with the neighboring molecule, indicating that this dent in the molecule is influenced by crystal packing (Figure 6).

In spite of the differences in the backbone torsion angles, the base-stacking configurations of the hexagonal structure are similar to the tetragonal (Figure 7). This is because of correlated variations in the backbone torsion angles that maintain the base-stacking geometries.

Local Base-Pair Parameters. A comparison of the two structures reveals that differences in the helical and base-pair parameters arise from the different distortions caused by crystal packing. The various base-pair parameters for the hexagonal and tetragonal structures are given in Table IV.

The tip angle of the terminal base pairs in the hexagonal structure shows a high value of 8°, probably because of the C2′-endo pucker of the penultimate sugar. This sugar pucker change rotates the δ (C4′–C3′) bond from gauche$^+$ to trans (Sundaralingam, 1969), swinging and tipping the terminal residue C8/C16 toward the major groove and thus increasing the tip angle. In the tetragonal structure, again larger tip angles in the opposite sense are seen at the ends of the duplex, which are apparently caused by the 12° kink in the center of the molecule. A similar kink is not observed in the hexagonal structure. The tip angles in the central region of both structures are small.

The inclination angle is generally higher in the hexagonal structure. The highest value for the A7 (A15) residues of 18° is probably again due to the C2′-endo sugar pucker, which increases the glycosyl-bond torsion angle χ and leads to an increase in the inclination angle. The roll angle displays an alternation in the hexagonal structure with a low value for the PuPy step and a high value for the PyPu step, consistent with Calladine's rules (Calladine, 1982) for an alternating sequence. The values show good agreement (Figure 8A) with the Calladine–Dickerson sum function Σ_2 (Dickerson, 1983). In the tetragonal octamer, at the central base-pair step the alternation is not pronounced, and the trend is broken, probably because of the kink.

The propeller twist also shows alternation in both the hexagonal and the tetragonal structures, with higher values for the G-C base pairs than the A-T base pairs (Figure 8B). The values are higher for the hexagonal structure at the ends and the central base-pair steps. This alternation is the reverse of the expected order. It is not clear if the extra Watson–Crick hydrogen bond has any bearing on this opposite trend. The bifurcated hydrogen bond between the purines G3 and A5 in the central region is about 3.2 Å in the hexagonal structure, similar to the tetragonal structure (3.1 Å) (Jain et al., 1989). The bifurcated hydrogen bonds between the purines (G1 and A15 and A7 and G9) at the ends of the duplex did not seem to occur, probably because of end effects.

The buckle angle, which is another measure of the noncoplanarity, shows a high value for the terminal base pair in both structures. These high values may be a consequence of optimizing the stacking interactions of the terminal base pairs with the sugar–phosphate backbone of symmetry-related molecules. The usually high buckle angle (19°) of the penultimate A-T base pairs of the hexagonal structure is due to the high glycosyl torsion angle of A7 (A15), associated with the C2′-endo sugar pucker.

The *x*-displacement shows significant variations in the hexagonal structure with higher values for the central base pairs, representing the more A-DNA-like characteristics of this form. Toward the ends, the displacement is diminished, presumably due to the distortion in the backbone at A7 (A15). In the tetragonal structure the *x*-displacements are uniformly low.

The twist angles are in accord with Calladine's rules for an alternating PuPy structure with higher values for the PuPy steps and lower values for the PyPu steps, with the exception

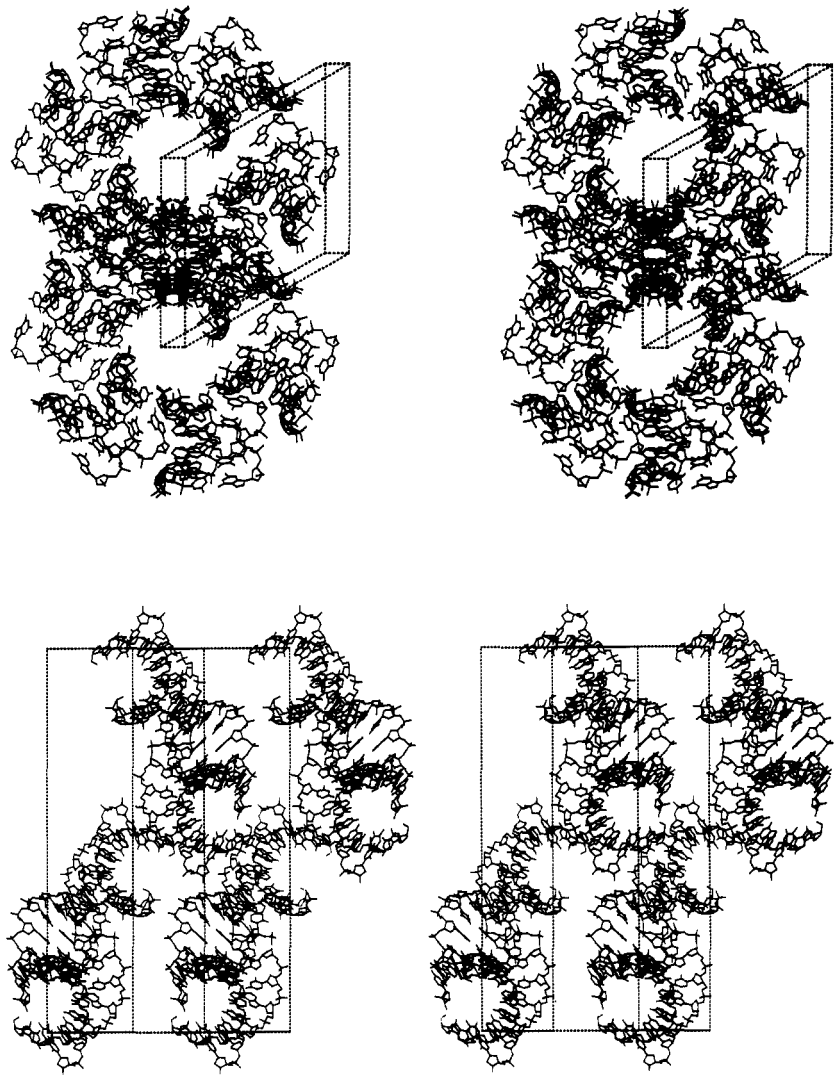

FIGURE 9: Stereoviews of the new crystal packing in the hexagonal structure. (Top) Looking down the *c* axis, showing the small water channel around the 6_1 screw axis. (Bottom) A view perpendicular to the above, showing the contacts between symmetry-related molecules.

of the ends (Figure 8C). For some unknown reason, the amplitude of the variation is dampened in the hexagonal structure, except in the terminal base-pair step. A structural explanation may be offered for the large twist angle in the latter. The C2′-endo sugar pucker of the penultimate sugar orients the C3′–O3′ bond axially (instead of equatorially), and this necessitates the large twist angle of the terminal base-pair step in order to optimize base stacking (Figure 7).

Crystal Packing. The crystal packing for the hexagonal structure is shown in two views in Figure 9. This is a novel packing for a hexagonal structure. Although the packing interactions are different in the two crystal forms (Jain & Sundaralingam, 1989), they have a fundamental similarity in that the terminal base pairs in both cases stack against the minor-groove sugar–phosphate of a symmetry-related duplex. This crystal-packing geometry is an invariant feature of all oligomers that have crystallized in the A-form and is thought to be responsible for inducing and stabilizing the A-conformation in the crystal.

Conclusion. Many of the differences in the two duplexes can be explained by the packing differences, which are responsible for distortions at different locations of the duplexes [see also Jain and Sundaralingam (1989)]. It is of interest that a C2′-endo residue has been accommodated within an A-DNA duplex, which provides stereochemical information of juxtaposed C2′-endo and C3′-endo sugar puckers. This would also be relevant to RNA structures. When the hexagonal structure is superimposed on the tetragonal structure, it is seen that the spermine molecule can be accommodated in the deep groove with minor changes in the torsion angles. The lack of binding of spermine is not readily apparent to us, although it may be due to the large deformation at the penultimate nucleotide pairs, which reduces the affinity of spermine by not allowing it to interact optimally with the terminal base pairs via water molecules.

The conformation of nucleotide units shows the preferred conformations for the nucleotides themselves. It is seen that much of the conformational latitudes in the nucleotides themselves are expressed in the conformational flexibility of the double helix.

The octamer d(GTGTACAC) assumes the A-DNA conformation apparently only in the solid state. Our solution circular dichroism studies indicate that the octamer occurs in the B-conformation (unpublished results). Similarly, NMR studies have revealed that the octamer adopts a B-DNA conformation in solution (Zehfus and Markley, personal communication). Thus, apparently spermine binding can be accommodated only in the A-conformation and not in the B-conformation. In fact, our model building (Jain & Sundaralingam, unpublished) with FRODO on a PS 300 molecular graphics system showed that the elongated B-DNA conformation does not permit binding of spermine to the bases only.

REFERENCES

Altona, C., & Sundaralingam, M. (1972) *J. Am. Chem. Soc. 94*, 8205-8212.

Brown, T., Hunter, W. N., Kneale, G., & Kennard, O. (1986) *Proc. Natl. Acad. Sci. U.S.A. 83*, 2402-2406.

Calladine, C. R. (1982) *J. Mol. Biol. 161*, 343-352.

Chambers, J. L., & Stroud, R. M. (1977) *Acta Crystallogr. B33*, 1824-1837.

Dickerson, R. E. (1983) *J. Mol. Biol. 166*, 419-441.

Di Gabriele, A. D., Sanderson, M. R., & Steitz, T. A. (1989) *Proc. Natl. Acad. Sci. U.S.A. 86*, 1816-1820.

EMBO Workshop (1989) *EMBO J. 8*, 1-4.

Fairall, L., Martin, S., & Rhodes, D. (1989) *EMBO J. 8*, 1809-1817.

Haran, T. E., Shakked, Z., Wang, A. H.-J., & Rich, A. (1987) *J. Biomol. Struct. Dyn. 5*, 199-217.

Heinemann, U., Lauble, H., Frank, R., & Blocker, H. (1987) *Nucleic Acids Res. 22*, 9531-9550.

IUPAC-IUB Joint Commission on Biochemical Nomenclature (1983) *Eur. J. Biochem. 131*, 9-15.

Jain, S., & Sundaralingam, M. (1989) *J. Biol. Chem. 264*, 12780-12784.

Jain, S., Zon, G., & Sundaralingam, M. (1987) *J. Mol. Biol. 197*, 141-145.

Jain, S., Zon, G., & Sundaralingam, M. (1989) *Biochemistry 28*, 2360-2364.

Jones, T. A. (1985) *Methods Enzymol. 115*, 157-171.

Rubin, J. R., Brennan, T., & Sundaralingam, M. (1972) *Biochemistry 11*, 3112-3128.

Sundaralingam, M. (1969) *Biopolymers 7*, 821-860.

Sundaralingam, M. (1973) *Jerusalem Symp. Quantum Chem. Biochem. 5*, 417-456.

Sundaralingam, M. (1982) in *Conformation in Biology* (Srinivasan, R., & Sarma, R. H., Eds.) pp 191-225, Adenine Press, New York.

Wang, A. H.-J., Quigley, G. J., Kolpak, F. J., Crawford, J. L., van Boom, J. H., van der Marel, G., & Rich, A. (1979) *Nature 282*, 680-686.

Wang, A. H.-J., Fuji, S., van Boom, J. H., & Rich, A. (1982) *Proc. Natl. Acad. Sci. U.S.A. 79*, 3968-3972.

Westhof, E., Dumas, P., & Moras, D. (1985) *J. Mol. Biol. 184*, 119-145.

Zon, G. (1990) in *HPLC in Biotechnology* (Hancock, W. S., Ed.) pp 301-397.

Mechanistic Stoichiometry of Mitochondrial Oxidative Phosphorylation†

Peter C. Hinkle,* M. Arun Kumar, Andrea Resetar, and David L. Harris

Section of Biochemistry, Molecular, and Cell Biology, Cornell University, Ithaca, New York 14853

Received August 27, 1990; Revised Manuscript Received January 17, 1991

ABSTRACT: P/O ratios of rat liver mitochondria were measured with particular attention to systematic errors. Corrections for energy loss during oxidative phosphorylation were made by measurement of respiration as a function of mitochondrial membrane potential. The corrected values were close to 1, 0.5, and 1 at the three coupling sites, respectively. These values are consistent with recent measurements of mitochondrial proton transport.

Eleven years ago, we reported that measured stoichiometries of mitochondrial oxidative phosphorylation were significantly lower than the traditional values of 1 per coupling site (Hinkle & Yu, 1979). Early studies of P/O ratios usually yielded values less than 1 per site, but it was assumed that the value was an integer and the results were described as "approaching" the now classical integers of 2 with succinate and 3 with NADH-linked substrates. Our observations that the P/O ratio with succinate as substrate is close to 1.5 have been confirmed by four research groups (Van Dam et al., 1980; Stoner, 1987; Hafner & Brand, 1988; Luvisetto & Azzone, 1989). Other groups have found slightly higher values (Beavis & Lehninger, 1986; Lemasters, 1984). When individual coupling sites are measured, there is agreement that site 2 forms less than 1 ATP per electron pair (Brand et al., 1978; Pozzan et al., 1979, Stoner, 1987), the value probably being 0.5, but there is less agreement about sites 1 and 3 [for reviews, see Hinkle and Yu (1979), Stoner (1987), and Lemasters et al. (1984)].

Chemiosmotic theory (Mitchell, 1965) provides a rationale for fractional values of P/O ratios because the proton is the coupling currency and the number of protons transported by a coupling region (site) of the respiratory chain need not be an integral multiple of the protons needed to synthesize ATP from ADP and P_i. Since ATP synthesis is measured in the external medium, ATP efflux and ADP plus P_i influx across the inner membrane must also occur, and these have been shown to be coupled to the influx of one proton, electrically, as ADP^{3-}/ATP^{4-} antiport and, chemically, as P_i^-/OH^- antiport (Klingenberg & Rottenberg, 1977). The use of protons to drive ATP/ADP + P_i transport and the leakage of protons across the mitochondrial inner membrane would lower the observed P/O ratio, although the protons used in transport are considered a part of the ideal "mechanistic" stoichiometry, whereas the "leak" protons or other mechanisms of energy loss are not.

We report here measurements of P/O ratios made with particular attention to several common systematic errors, and other measurements to estimate energy losses during oxidative phosphorylation. It is concluded that ideal mechanistic stoichiometries are 1.0 at sites 1 and 3, and 0.5 at site 2, values suggested previously (Hinkle, 1981).

EXPERIMENTAL PROCEDURES

Rat liver mitochondria were prepared in 250 mM sucrose with two washes (Pederson et al., 1978). Many variations in the preparation were tried, and while respiratory control and respiration rates depended on the method, the P/O values were very insensitive to the details of the procedure. The standard medium for measurements reported was 250 mM sucrose, 10 mM K-MOPS (pH 7.2), 5 mM KP_i (pH 7.2), 5 mM $MgCl_2$,

† This work was supported by NIH Grant HL 14483.

0006-2960/91/0430-3576$02.50/0